JASCO APPLIED SCIENCES

8630 Fenton Street, Suite 218
Silver Spring, MD 20910 USA

Tel: +1-301-565-3500
www.jasco.com

Memo

DATE: 26 September 2022

FROM: M. Weirathmueller, K. Zammit, M. Koessler, D. Zeddies (JASCO Applied Sciences (USA) Inc.)

TO: Benjamin Laws and Jolie Harrison (National Oceanic and Atmospheric Administration)

Subject: Gulf of Mexico Exposure Estimation

This document describes the methodology that was employed in predicting the number of marine mammals that may be exposed to sound levels exceeding thresholds for injury or behavioral disturbance resulting from geophysical survey activities in the Gulf of Mexico.

1. Overview

The current modeling effort included the following updates:

- Updates to all species behavioral definition files for animal movement and exposure modeling
- Marine mammal densities were updated for most species using the most recently available densities from the National Marine Fisheries Service's Southeast Fisheries Science Center (SEFSC)
- The addition of a 5110 in^3 seismic airgun array

2. Sound source modeling

The source levels and directivity of seismic sources were predicted with JASCO's Airgun Array Source Model (AASM). AASM includes low- and high-frequency modules for predicting different components of the seismic source spectrum. The low-frequency module is based on the physics of oscillation and radiation of airgun bubbles, as originally described by Ziolkowski (1970), that solves the set of parallel differential equations that govern bubble oscillations. Physical effects accounted for in the simulation include pressure interactions between airguns, port throttling, bubble damping, and generator-injector (GI) gun behavior discussed by Dragoset (1984), Laws et al. (1990), and Landrø (1992). A global optimization algorithm tunes free parameters in the model to a large library of airgun source signatures.

While airgun signatures are highly repeatable at the low frequencies, which are used for seismic imaging, their sound emissions have a largely random component at higher frequencies that cannot be predicted using a deterministic model. Therefore, AASM uses a stochastic simulation to predict the high-frequency (800−25,000 Hz) sound emissions of individual airguns, using a data-driven multiple-regression model. The multiple-regression model is based on a statistical analysis of a large collection of high quality

seismic source signature data recently obtained from the Joint Industry Program (JIP) on Sound and Marine Life (Mattsson and Jenkerson 2008). The stochastic model uses a Monte-Carlo simulation to simulate the random component of the high-frequency spectrum of each airgun in an array. The mean high-frequency spectra from the stochastic model augment the low-frequency signatures from the physical model.

AASM produces a set of "notional" signatures for each array element based on:

- Array layout
- Volume, tow depth, and firing pressure of each airgun
- Interactions between different airguns in the array

In addition to the previously modeled, 8000 in^3 and 4130 in^3 seismic sources, a 5110 in^3 seismic source was modeled. Figure 1 shows the array layout of the 5110 in^3 source, the intended tow depth is 12 m. The layout is presented in a nominal cartesian coordinate system, with the direction of vessel travel (tow direction) along the positive X-axis and the array centered on the X-Y origin.

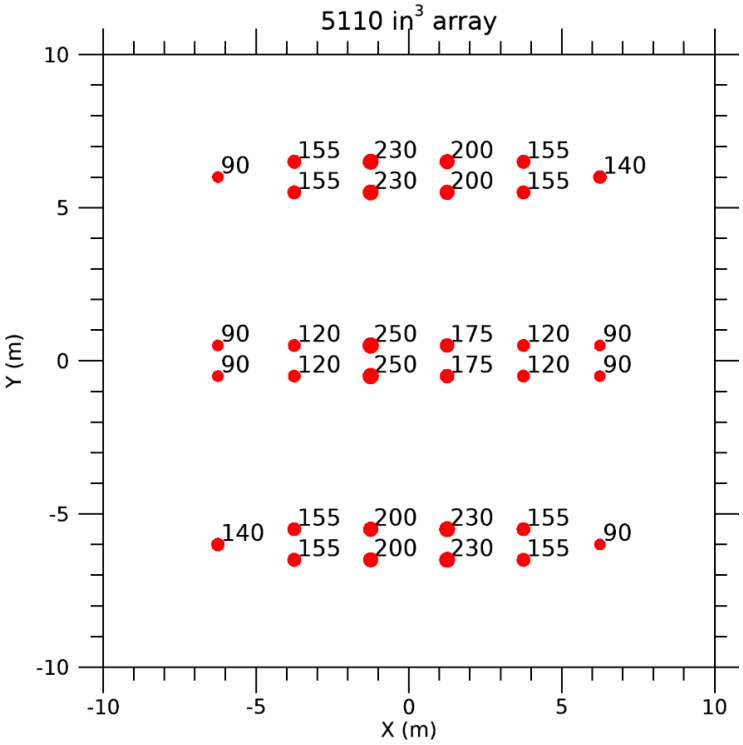

Figure 1. Layout of the modeled 5110 in^3 seismic source where the plotted layout is such that the array is centered on the origin and vessel travel direction is in the positive x-direction. Tow depth is 12 m. The labels indicate the firing volume (in cubic inches) for each airgun. Firing pressure for all guns was 2000 psi.

3. Sound propagation

Long-range sound fields were computed using JASCO's Marine Operations Noise Model (MONM) and JASCO's Full Waveform Range-dependent Acoustic Model (FWRAM). MONM was used to predict results for per-pulse SEL metrics and FWRAM was used to predict results for SPL and PK metrics. The source and propagation modeling approaches remain the same as for the previous modeling effort.

3.1. MONM

MONM was used to compute sound propagation at frequencies between 10 Hz to 2 kHz via a wide-angle parabolic equation solution to the acoustic wave equation (Collins 1993) based on a version of the US Naval Research Laboratory's Range-dependent Acoustic Model (RAM), which has been modified to account for a solid seabed (Zhang and Tindle 1995). MONM treats frequency dependence by computing acoustic propagation loss at the center frequencies of decidecade bands.

The parabolic equation method has been extensively benchmarked and is widely employed in the underwater acoustics community (Collins et al. 1996). MONM accounts for the additional reflection loss at the seabed, which results from partial conversion of incident compressional waves to shear waves at the seabed and sub-bottom interfaces, and it includes wave attenuations in all layers. MONM incorporates the following site-specific environmental properties: a bathymetric grid of the modeled area, underwater sound speed as a function of depth, and a geoacoustic profile based on the overall stratified composition of the seabed.

MONM computes acoustic fields by modeling propagation loss within two-dimensional (2-D) vertical planes aligned along number of planes (Figure 2) covering a swath of angles from the source, an approach commonly referred to as N×2-D.

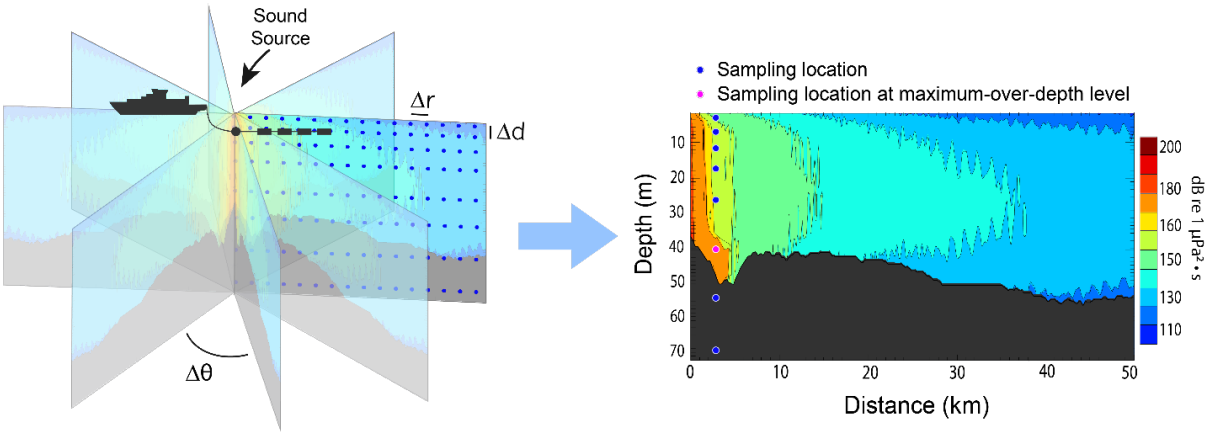

Figure 2. The N×2-D approach used by MONM.

Sufficiently many decidecade bands, starting at 10 Hz, are modeled to include most of the acoustic energy emitted by the seismic source. At each center frequency, the propagation loss is modeled within each of the N vertical planes as a function of depth and range from the source. The decidecade band received per-pulse SEL are computed by subtracting the band propagation loss values from the directional source level in that frequency band. Composite broadband received per-pulse SEL are then computed by summing the received decidecade band levels.

3.2. Full Waveform Range-dependent Acoustic Model: FWRAM

The per-pulse SEL of sound pulses is an energy-like metric related to the dose of sound received over a pulse's entire duration. The pulse SPL on the other hand, is related to its intensity over a specified time interval. For impulsive sounds from the seismic source, time-domain representations of the pressure waves are required to calculate SPL and PK metrics. Furthermore, the seismic source must be represented as a distributed source to accurately characterise vertical directivity effects in the near-field zone, which is important for PK predicitions. Synthetic pressure waveforms were computed using FWRAM, which is a time-domain acoustic model based on the wide-angle parabolic equation (PE) algorithim. FWRAM computes pressure waveforms via Fourier synthesis of the modeled acoustic transfer function in closely spaced frequency bands. Furhtermore, JASCO's FWRAM model computes synthetic pressure waveforms versus range and depth for range-varying marine acoustic environments, including bathymetry, water sound speed profile, and seafloor geoacoustic profile. FWRAM employs the array starter method to accurately model sound propagation from a spatially distributed source (MacGillivray and Chapman 2012).

The synthetic waveforms from FWRAM were used to convert the MONM SEL results to SPL. Fourier synthesis modeling can be computationally intensive and predicting SPL for all modeled radials can be prohibitively time consuming when run at high spatial resolution over large areas. Full-waveform modeling was used to estimate SPL at a subset of radial planes, the closest ones were used to convert the SEL values from MONM to SPL.

3.3. Sound fields

Figure 3 shows the single-shot SEL sound fields produced by the three seismic sources. The sound fields produced by the arrays are complex and determined by the specific configuration of the arrays and their tow depth. The depth at which a source is placed influences the interference pattern caused by the direct and sea-surface reflected paths, commonly referred to as the "Lloyd mirror pattern". The destructive interference from the sea-surface reflection ("ghost") is generally greater for shallow tow depths compared to deeper tow depths. The 5110 in^3 array was modelled at 12 m depth while the other two arrays were modelled at 8 m. In Figure 3, the isopleth to single shot SEL 143 dB re 1 $\mu Pa^2 \cdot s$ is highlighted (red contour) for the three arrays and shows that the ensonified areas are not symmetric. It can also be seen that while the 8000 in^3 array does have the longest ranges, it does not necessarily have the largest affected area. It is the affected area (more precisely, volume) that drives the exposure estimates. (Note that the isopleths do not show the additional complexity that exists in the vertical dimension).

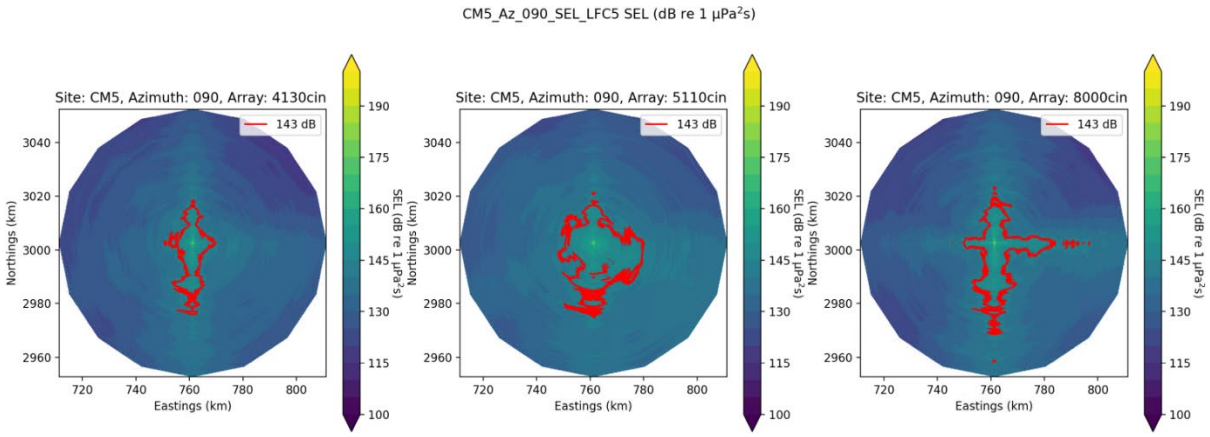

Figure 3. SEL sound field produced by single shots of the 4130, 5110, and 8000 in^3 seismic sources. A single contour (red line) is included for comparative purposes. This example contour corresponds to an SEL of 143 dB re 1 µPa^2·s. Vessel travel direction (tow direction) is east.

4. Animal movement modeling

Animal movement and exposure modeling was done using JASCO's Animal Simulation Model Including Noise Exposure (JASMINE). JASMINE was used to estimate the probability of exposure of animals to sound arising from expected seismic surveys. Sound exposure models such as JASMINE use simulated animals (animats) to sample the modeled 3-D sound fields with movement rules derived from animal observations (see Figure 4). Previous animal movement and exposure modeling used the Marine Mammal Movement and Behavior model (3MB) developed by Houser (2006). The animal movement part of the JASMINE model is based on 3MB. JASMINE additionally incorporates sound fields into the model rather than combining the animat tracks and sound fields afterwards. While the implementation has been improved and expanded, the core functionality remains the same.

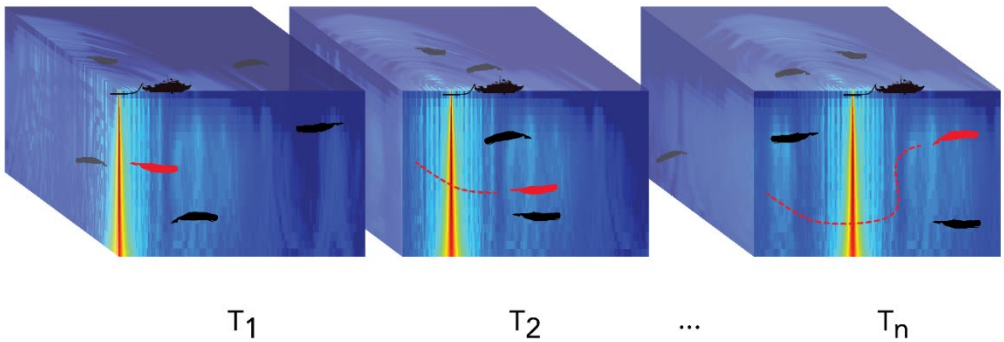

Figure 4. Depiction of animats in an environment with a moving sound field. Example animat (red) shown moving with each time step. The acoustic exposure of each animat is determined by where it is in the sound field, and its exposure history is accumulated as the simulation steps through time.

The parameters used for forecasting realistic behaviors (e.g., diving, foraging, and surface times) were determined and interpreted from marine species studies (e.g., tagging studies) where available, or reasonably extrapolated from related species. Time-varying, three-dimensional sound fields were sampled by the model receivers in a way that real animals are expected to by programming animats to

behave like marine species that may be present. The output of the simulation is the exposure history for each animat within the simulation. An individual animat's sound exposure levels are summed over a specific duration, i.e., 24 h, to determine its total received acoustic energy (SEL) and maximum received PK and SPL. These received levels are then compared to the threshold criteria for injury and behavioral response.

Animal movement modeling was conducted for each species in each of the BOEM Gulf of Mexico management areas as shown in Figure 5.

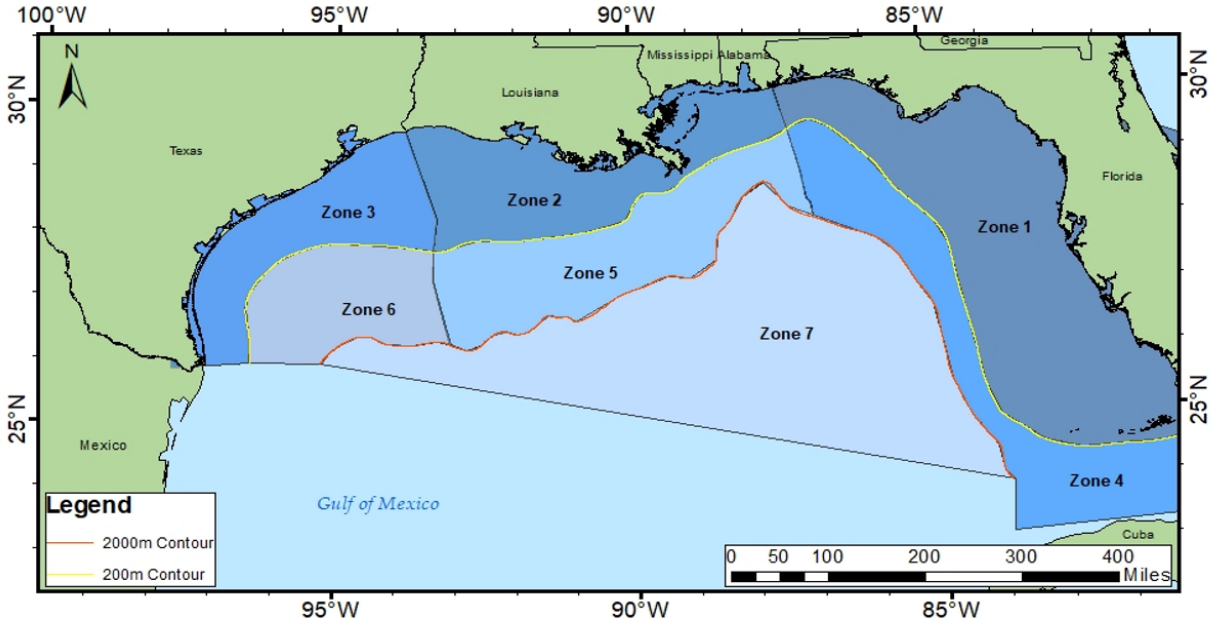

Figure 5. BOEM Gulf of Mexico management areas, shown as Zones 1–7.

The survey types included in this modeling effort are the same as the previous modeling, and include: 3D narrow azimuth, 3D wide azimuth, 2-Dimensional, and Coil. The seismic array sizes included: 4130 in^3, 5110 in^3, and 8000 in^3.

Marine mammal species that may be expected in the GoM were considered, and the following species modeled:

- Rice's whale
- Atlantic spotted dolphin
- Blainville's beaked whale
- Bottlenose dolphin
- Clymene dolphin
- Cuvier's beaked whale
- False killer whale
- Fraser's dolphin
- Gervais' beaked whale
- Killer whale
- Melon-headed whale
- Pantropical spotted dolphin
- Pygmy killer whale
- Risso's dolphin
- Rough-toothed dolphin

- Short-finned pilot whale
- Sperm whale
- Spinner dolphin
- Striped dolphin
- Dwarf sperm whale
- Pygmy sperm whale

For the current modeling effort, all species definition parameters were updated according to the most recent literature. This is an ongoing process that requires review at the start of all new and reopened modeling efforts. Changes implemented include minimum and maximum seeding depth, travel rate, and new dive profiles. The seeding depth limits are used to specify where the animats are placed spatially during simulations. Changes in seeding depth can result in substantial differences in exposures. Figures 6 and 7 show example comparisons of seeding depth for the original modeling effort and seeding depth for the recent modeling effort for kogia and Rice's whales in Zone 5.

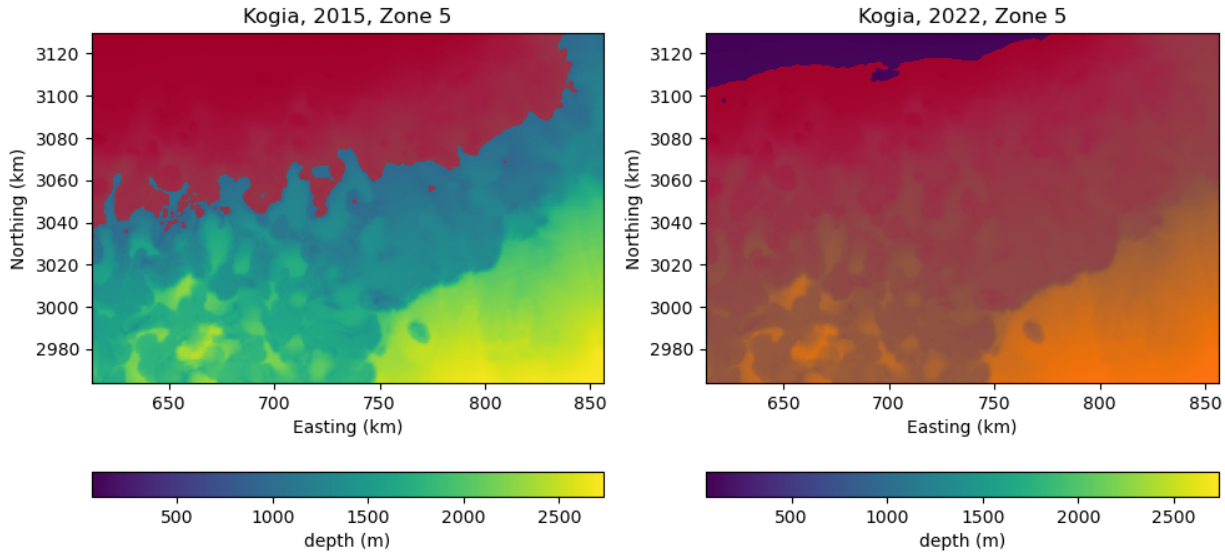

Figure 6.Seeded area for kogia within Zone 5, show in transparent red, overlaid on the bathymetry. The seeding area for the original modeling is show in the left panel and the seeding area for the recent modeling is shown in the right panel.

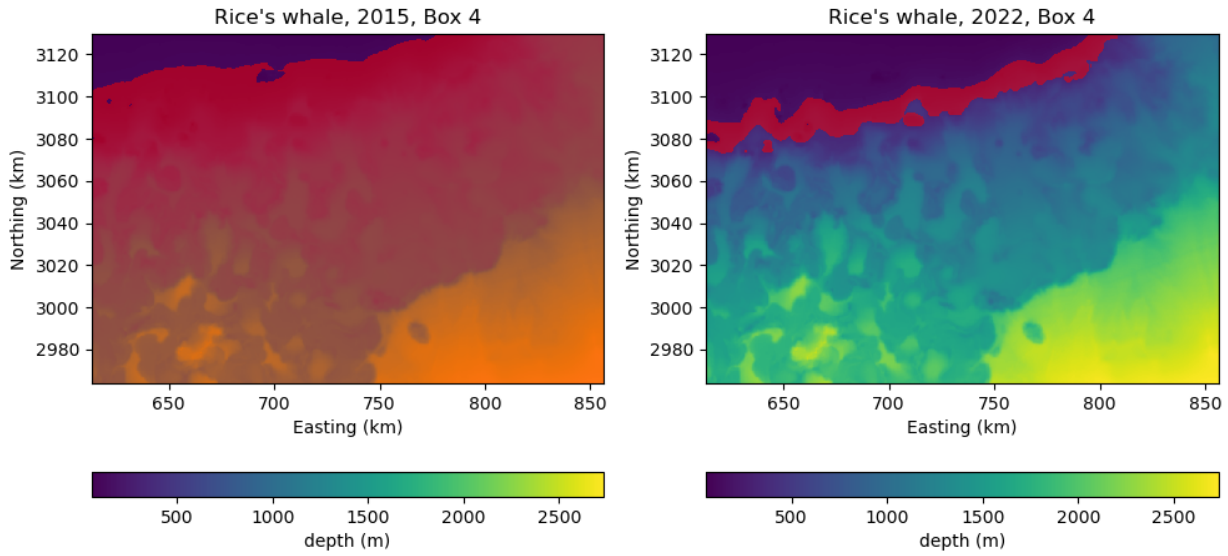

Figure 7.Seeded area for Rice's whales within Zone 5, show in transparent red, overlaid on the bathymetry. The seeding area for the original modeling is show in the left panel and the seeding area for the recent modeling is shown in the right panel.

5. Marine mammal density

Mean monthly marine mammal density (animals per 100 square kilometers [animals/100 km^2]) was estimated for all species for each of the BOEM Gulf of Mexico Management Areas. Preliminary density data were obtained from the Southeast Fisheries Science Center (SEFSC). Densities were calculated for each species as the average value within all cells either partially or fully within each of the zones. A summary of the changes in animal density are included in Appendix A.

In certain cases, densities were presented for guilds, where the density values represented more than one species. The two guilds were kogia, which included pygmy and dwarf sperm whales, and blackfish, which included melon-headed whales, killer whales, false killer whales, and pygmy killer whales. Since each of the sub-species within these guilds was run separately within JASMINE, exposure estimates are provided for each. The species within each guild were scaled using the full guild density.

6. Exposure calculations

Animal movement modeling was used to predict exposures in 24-hour time periods during each of the survey types. The 24-hr exposure estimates were then scaled by the animal density and the anticipated level of effort over a 5-year period. A summary of the predicted exposures for each zone and survey type are provided in Appendix B.

NMFS determined that the potential for Level A harassment of mid-frequency cetaceans is de minimis (see 86 FR 5354). Therefore, the final exposure predictions do not include incidents of Level A harassment for that hearing group. Exposure estimates for Level A and Level B were obtained independently of each other, and no potential exposures above behavioral criteria were omitted.

7. Discussion

Exposure estimates for several different survey types (3D narrow azimuth, 3D wide azimuth, 2D, and Coil) were obtained for three different seismic arrays (4130, 5110, and 8000 in^3) (shown in Appendix B). In general, behavioral exposure estimates increase as the array volume increases but not in all cases. For example, the Rice's whale behavioral exposures for the 5110 in^3 array are greater than the 8000 in^3 array. Injury exposures for kogia were typically higher for the 5110 in^3 array than the 4130 in^3 array but decreased from 5110 in^3 to 8000 in^3.

While the 8000 in^3 array does have the longest absolute ranges, the 5110 in^3 array has similar, or greater, ensonified area (Section 3.3). Though an important factor, array volume is not necessarily the best indicator of potential impacts – the configuration and use of the array (e.g., tow depth) determine the sound production and directivity pattern of the sound field, and potential for exposures.

Exposure estimates generated from this modeling work are based on best currently available data. Animal density estimates were obtained from the NMFS Southeast Fisheries Science Center model results (unpublished data from NMFS-SEFSC, 2022) and species definitions were updated based on published data.

Collins, M.D. 1993. A split-step Padé solution for the parabolic equation method. *Journal of the Acoustical Society of America* 93(4): 1736-1742. https://doi.org/10.1121/1.406739.

Collins, M.D., R.J. Cederberg, D.B. King, and S. Chin-Bing. 1996. Comparison of algorithms for solving parabolic wave equations. *Journal of the Acoustical Society of America* 100(1): 178-182. https://doi.org/10.1121/1.415921.

Dragoset, W.H. 1984. A comprehensive method for evaluating the design of airguns and airgun arrays. *16th Annual Offshore Technology Conference* Volume 3, 7–9 May 1984. OTC 4747, Houston, TX, USA. pp. 75–84. https://doi.org/10.4043/4783-MS.

Houser, D.S. 2006. A method for modeling marine mammal movement and behavior for environmental impact assessment. *IEEE Journal of Oceanic Engineering* 31(1): 76-81. https://doi.org/10.1109/JOE.2006.872204.

Landrø, M. 1992. Modeling of GI gun signatures. *Geophysical Prospecting* 40(7): 721–747. https://doi.org/10.1111/j.1365-2478.1992.tb00549.x.

Laws, R.M., L. Hatton, and M. Haartsen. 1990. Computer modelling of clustered airguns. *First Break* 8(9): 331–338. https://doi.org/10.3997/1365-2397.1990017.

MacGillivray, A.O. and N.R. Chapman. 2012. Modeling underwater sound propagation from an airgun array using the parabolic equation method. *Canadian Acoustics* 40(1): 19-25. https://jcaa.caa-aca.ca/index.php/jcaa/article/view/2502/2251.

Mattsson, A. and M. Jenkerson. 2008. Single Airgun and Cluster Measurement Project. *Joint Industry Programme (JIP) on Exploration and Production Sound and Marine Life Proramme Review*. 28-30 Oct 2008. International Association of Oil and Gas Producers, Houston, TX, USA.

Zhang, Z.Y. and C.T. Tindle. 1995. Improved equivalent fluid approximations for a low shear speed ocean bottom. *Journal of the Acoustical Society of America* 98(6): 3391-3396. https://doi.org/10.1121/1.413789.

Ziolkowski, A.M. 1970. A method for calculating the output pressure waveform from an air gun. *Geophysical Journal International* 21(2): 137-161. https://doi.org/10.1111/j.1365-246X.1970.tb01773.x.

Appendix A. Animal densities

Animal densities were updated for the recent modeling effort. Table A-1 shows the percent change from the 2015 densities to the 2022 densities. Note that many of the very high percentage values (e.g., Clymene dolphin in zones 2 and 3) are due to previous densities being extremely low.

Table A-1. Percent change in animal density for each species and zone, from 2015 to 2022.

Species	Zone 1	Zone 2	Zone 3	Zone 4	Zone 5	Zone 6	Zone 7
Rice's whale	29%	3599%	9872%	74%	71%	104%	20755%
Dwarf sperm whale	-99%	23%	751%	-92%	-75%	-53%	17%
Pygmy sperm whale	-99%	23%	751%	-92%	-75%	-53%	17%
Atlantic spotted dolphin	-84%	-80%	-73%	-96%	-84%	83%	782%
Blainville's beaked whale	-95%	1012%	2391%	-85%	-87%	-83%	-62%
Bottlenose dolphin	-32%	-22%	-22%	-41%	-68%	-37%	-61%
Clymene dolphin	-50%	164588 %	4022010 %	-67%	-82%	-62%	-58%
Cuvier's beaked whale	-95%	1012%	2391%	-85%	-87%	-83%	-62%
False killer whale	-97%	-35%	95%	62%	115%	146%	138%
Fraser's dolphin	4%	157%	395%	-1%	1%	-1%	0%
Gervais' beaked whale	-95%	1012%	2391%	-85%	-87%	-83%	-62%
Killer whale	915%	10522%	13398%	8787%	7655%	9052%	2190%
Melon-headed whale	48%	10274%	41299%	0%	-29%	-4%	16%
Pantropical spotted dolphin	-88%	1398%	6989%	-63%	-59%	-48%	-51%
Pygmy killer whale	217%	23899%	89473%	298%	242%	280%	170%
Risso's dolphin	-97%	303%	374%	-79%	-72%	-72%	-68%
Rough-toothed dolphin	1%	8%	6%	-3%	1%	0%	3%
Short-finned pilot whale	236%	83551%	1001290 %	-52%	-32%	2%	104%
Sperm whale	12%	16937%	41523%	-17%	-44%	-15%	-12%
Spinner dolphin	-96%	156265 %	1150568 %	-93%	-95%	-98%	-58%
Striped dolphin	148%	38308%	20930%	235%	-1%	-41%	69%

Appendix B. ITR Results Summary

Total predicted exposures are included for each survey type and zone in Tables B-**2** - B-**3** using the 5-year effort schedule described in Table B-1. The animal movement modeling simulations produced daily exposure estimates for each month of the year since that was the resolution of the density data. The effort schedule obtained from the original ITR provided total projected number of days of effort per year. The yearly effort was divided equally into 12 months to match the exposure estimate resolution. Since partial survey days are incompatible with the 24-hour time steps considered using JASMINE, any partial effort days were rounded up to the nearest integer.

Table B-1. Projected levels of effort in 24-h survey days for 5 years, by zone and survey type.

Year	Zone	2D	3D-NAZ	3D-WAZ	COIL
1	1	0	0	0	0
	2	0	240	0	0
	3	0	36	0	0
	4	0	0	0	0
	5	60	384	192	84
	6	0	192	60	24
	7	48	348	168	72
2	1	0	0	0	0
	2	0	360	48	24
	3	0	0	0	0
	4	12	0	0	0
	5	0	384	192	84
	6	0	108	0	0
	7	24	336	168	72
3	1	0	0	0	0
	2	0	240	0	0
	3	0	0	0	0
	4	0	0	0	0
	5	0	336	156	72
	6	0	192	60	24
	7	0	312	144	60
4	1	0	0	0	0
	2	0	360	48	24
	3	0	36	0	0
	4	12	12	0	0
	5	36	240	96	48
	6	0	108	0	0
	7	72	264	96	48
5	1	0	0	0	0
	2	0	240	0	0
	3	0	0	0	0
	4	0	24	0	0
	5	0	288	192	84
	6	0	108	0	0
	7	0	324	168	72

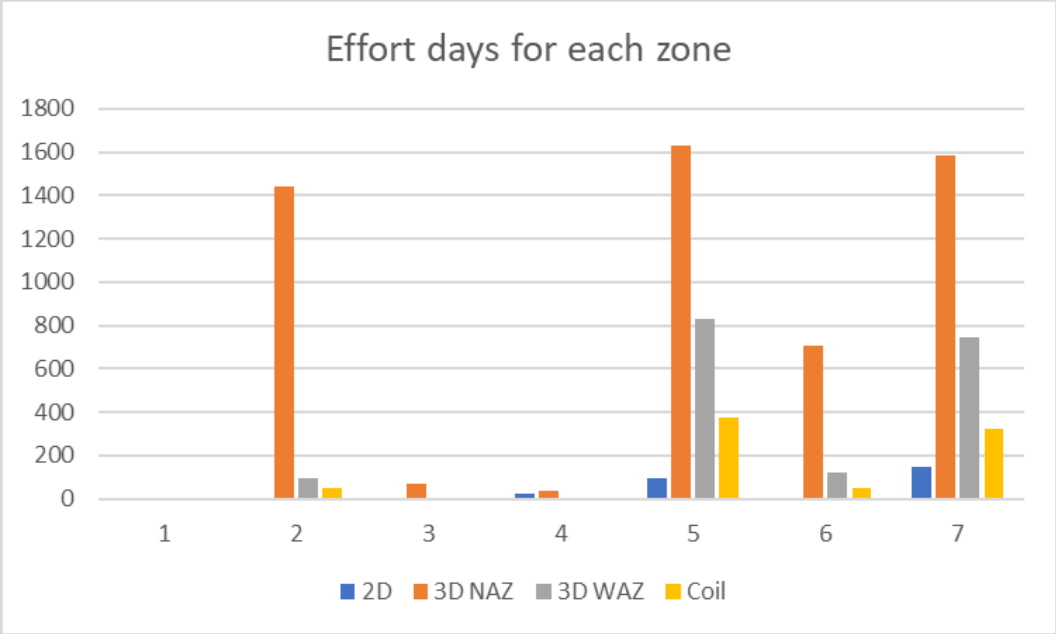

Figure B-1. Plot showing the number of 24-h survey days for each zone and survey type, summed over all 5 years of predicted effort.

Table B-2. Total exposures, summed over all five years, for the 4130 in3 array for all survey types.

Species	2D		3D NAZ		3D WAZ		COIL	
	Level A	Level B	Level A	Level B	Level A	Level B	Level A	Level B
Rice's whale	0.0	8.6	0.3	66.1	0.0	20.9	0.0	6.7
Dwarf sperm whale	71.6	695.0	2070.1	13401.9	1713.4	6302.2	655.7	2085.4
Pygmy sperm whale	71.6	695.0	2070.1	13401.9	1713.4	6302.2	655.7	2085.4
Atlantic spotted dolphin	0.0	654.1	0.0	111247.0	0.0	15275.0	0.0	6438.6
Blainville's beaked whale	0.0	2684.7	0.0	57536.2	0.0	29014.3	0.0	8862.6
Bottlenose dolphin	0.0	3909.7	0.0	1248538.3	0.0	97005.3	0.0	35151.7
Clymene dolphin	0.0	2694.8	0.0	64491.2	0.0	26396.0	0.0	8436.5
Cuvier's beaked whale	0.0	2865.8	0.0	60036.2	0.0	29746.0	0.0	9025.9
False killer whale	0.0	6912.6	0.0	145718.8	0.0	61098.5	0.0	22332.9
Fraser's dolphin	0.0	1481.5	0.0	31289.2	0.0	12413.6	0.0	5372.4
Gervais' beaked whale	0.0	2684.7	0.0	57536.2	0.0	29014.3	0.0	8862.6
Killer whale	0.0	6695.1	0.0	147012.4	0.0	58873.9	0.0	25189.3
Melon-headed whale	0.0	6092.1	0.0	132534.1	0.0	54221.1	0.0	21264.3
Pantropical spotted dolphin	0.0	34988.7	0.0	638155.7	0.0	267751.2	0.0	114309.0
Pygmy killer whale	0.0	6161.7	0.0	124788.4	0.0	55558.8	0.0	17517.7
Risso's dolphin	0.0	838.5	0.0	17430.9	0.0	7707.8	0.0	2350.2
Rough-toothed dolphin	0.0	3677.8	0.0	87121.0	0.0	32233.7	0.0	13533.0
Short-finned pilot whale	0.0	802.2	0.0	31409.3	0.0	10023.7	0.0	3354.2
Sperm whale	0.0	1495.7	0.0	29625.2	0.0	12554.7	0.0	3746.6
Spinner dolphin	0.0	721.7	0.0	9988.6	0.0	4746.3	0.0	1735.8
Striped dolphin	0.0	7177.1	0.0	123543.8	0.0	52987.5	0.0	23122.1

Table B-3. Total exposures, summed over all five years, for the 5110 in^3 array for all survey types.

Species	2D		3D NAZ		3D WAZ		COIL	
	Level A	Level B	Level A	Level B	Level A	Level B	Level A	Level B
Rice's whale	0.1	11.6	0.4	83.9	0.0	26.9	0.0	8.3
Dwarf sperm whale	79.8	763.5	2335.5	14708.7	1940.6	6931.5	716.5	2255.8
Pygmy sperm whale	79.8	763.5	2335.5	14708.7	1940.6	6931.5	716.5	2255.8
Atlantic spotted dolphin	0.0	668.9	0.0	119958.0	0.0	16060.5	0.0	6726.1
Blainville's beaked whale	0.0	2720.9	0.0	55810.1	0.0	28459.8	0.0	8755.6
Bottlenose dolphin	0.0	3854.1	0.0	1281505.0	0.0	98687.8	0.0	36058.0
Clymene dolphin	0.0	3060.5	0.0	69291.5	0.0	27983.4	0.0	8655.2
Cuvier's beaked whale	0.0	2980.2	0.0	60401.5	0.0	30124.4	0.0	8976.9
False killer whale	0.0	7603.8	0.0	153298.9	0.0	64187.1	0.0	22515.8
Fraser's dolphin	0.0	1629.1	0.0	32986.0	0.0	13197.3	0.0	5456.6
Gervais' beaked whale	0.0	2720.9	0.0	55810.1	0.0	28459.8	0.0	8755.6
Killer whale	0.0	7317.1	0.0	153814.2	0.0	61814.1	0.0	25543.2
Melon-headed whale	0.0	6783.7	0.0	140444.7	0.0	57757.4	0.0	21672.7
Pantropical spotted dolphin	0.0	39261.7	0.0	677526.8	0.0	290340.7	0.0	118284.2
Pygmy killer whale	0.0	6963.1	0.0	134273.4	0.0	59430.8	0.0	17714.0
Risso's dolphin	0.0	888.6	0.0	17960.4	0.0	7918.2	0.0	2384.1
Rough-toothed dolphin	0.0	4060.5	0.0	92473.4	0.0	34462.6	0.0	13891.0
Short-finned pilot whale	0.0	834.8	0.0	32897.6	0.0	10378.6	0.0	3445.6
Sperm whale	0.0	1664.4	0.0	31708.2	0.0	13529.7	0.0	3824.9
Spinner dolphin	0.0	745.4	0.0	9892.8	0.0	4776.7	0.0	1767.0
Striped dolphin	0.0	8106.7	0.0	132144.2	0.0	57584.2	0.0	23664.5

Table B-4. Total exposures, summed over all five years, for the 8000 in^3 array for all survey types.

Species	2D		3D NAZ		3D WAZ		COIL	
	Level A	Level B	Level A	Level B	Level A	Level B	Level A	Level B
Rice's whale	0.1	9.7	0.4	69.2	0.0	21.1	0.0	7.5
Dwarf sperm whale	64.0	863.5	1864.2	16146.6	1523.8	7544.9	604.5	2232.0
Pygmy sperm whale	64.0	863.5	1864.2	16146.6	1523.8	7544.9	604.5	2232.0
Atlantic spotted dolphin	0.0	792.6	0.0	135967.7	0.0	18492.9	0.0	7341.0
Blainville's beaked whale	0.0	3254.8	0.0	69608.9	0.0	35093.5	0.0	10118.5
Bottlenose dolphin	0.0	4733.2	0.0	1483454.2	0.0	115389.8	0.0	39500.8
Clymene dolphin	0.0	3155.4	0.0	74786.1	0.0	30507.0	0.0	9198.4
Cuvier's beaked whale	0.0	3408.3	0.0	71283.3	0.0	35418.0	0.0	10177.9
False killer whale	0.0	7975.5	0.0	167328.3	0.0	70118.5	0.0	24342.9
Fraser's dolphin	0.0	1749.5	0.0	36720.9	0.0	14568.1	0.0	5935.7
Gervais' beaked whale	0.0	3254.8	0.0	69608.9	0.0	35093.5	0.0	10118.5
Killer whale	0.0	7758.6	0.0	169909.2	0.0	68146.0	0.0	27489.1
Melon-headed whale	0.0	7093.0	0.0	152962.3	0.0	62703.4	0.0	23129.6
Pantropical spotted dolphin	0.0	41311.9	0.0	742971.0	0.0	313310.4	0.0	125311.7
Pygmy killer whale	0.0	7108.3	0.0	143162.3	0.0	63639.1	0.0	19033.3
Risso's dolphin	0.0	981.8	0.0	20311.7	0.0	8972.7	0.0	2615.2
Rough-toothed dolphin	0.0	4297.0	0.0	102610.9	0.0	37393.8	0.0	15015.3
Short-finned pilot whale	0.0	935.9	0.0	36515.7	0.0	11621.8	0.0	3752.9
Sperm whale	0.0	1725.7	0.0	33631.2	0.0	14277.5	0.0	4087.6
Spinner dolphin	0.0	857.5	0.0	11656.2	0.0	5593.4	0.0	1920.3
Striped dolphin	0.0	8498.7	0.0	144246.9	0.0	61836.2	0.0	25190.9